Chapter-4

Theoretical optimization of double dielectric back reflector layer for thin c-Si based advanced solar cells with notable enhancement in MAPD

CHAPTER CONTENTS

4.1 Introduction

4.2 Computational modeling and analyses

4.2.1 Optical Design

4.2.2 Modelling and Design Approximation

4.3 Results and discussions

4.3.1 Optimization of back reflector layers (BRLs)

4.3.2 Optoelectronic properties of the BRLs

4.3.3 Solar cell performance and parameters

4.4 Chapter Conclusion

4.1. Introduction

The recent trends in solar photovoltaics mainly address the use of thinner active layers in devices like dye-sensitized [209-211], organic [212-214], perovskite [215-217], inorganic-organic hybrid [218-220], quantum dot [221-223], quantum well [224-225], and thin crystalline silicon [226-228] based solar cells. Efficiency, cost-effectiveness, and durability are the primary concerns of current photovoltaic research. Though there is a series of advanced types of solar cell technologies, however, crystalline silicon (c-Si) based technology prevails in the domain due to its high stabilized efficiency, unparalleled reliability, and sustainability. On the other hand, due to indirect bandgap and low optical absorption [229], crystalline silicon-based conventional cells demand a high thickness of active layer like 150 to 180 μm, and this also enhances the cost of the device. However, *Shockley*, in his work [230-231], proved that a ~30 μm thick c-Si substrate is sufficient enough to make a solar cell. Still, some optical engineering is essential for such devices to achieve high efficiency. Optical engineering, mainly on the back surface of the active layer, is equally critical to most of the 'thinner' variation of solar cells [232-234]. Considering the ease of fabrication through the mainstream flow line, the possibility of commercialization, and the robustness of the device, thin c-Si based cells have drawn the attention of researchers over the other modern types of solar cells [235-238]. Two significant drawbacks of thin (~30 μm) crystalline silicon, namely (i) transmittance of light through the active Si layer in the longer wavelengths (700 nm onwards) and (ii) surface recombination due to the presence of dangling bonds/defects levels, must be dealt with care for the successful fabrication of such device. The former can be addressed by introducing a back reflector layer on the rear surface of the active c-Si layer. This back reflector layer should preferably be lossless. The latter can be solved by the use of a

‘passivation’ layer. The top side light management schemes are well established [239-240] and have not been considered in the present investigation. For rear side optical engineering in c-Si cells; *Feng* et.al [241] reported that incorporation of a diffractive Bragg grating on the backside could enhance the absorption of photons having a wavelength in the range 800–1100 nm in 2–10 µm thick c-Si wafers. *Heine* et al. reported that blazed grating on the back could increase the optical thickness of the wafer to a significant extent [242]. There are several reports on the use of dielectric Bragg reflectors (DBR) or DBR based nanostructures with dielectrics on the rear side of the cell for better light trapping and efficiency enhancement [243-246]. Materials like a-Si:H, indium tin oxide (ITO), SiNx, HfO_2, SiO_2, etc. are known to have significant application as DBR in various types of solar cells, like thin silicon cells, multiple quantum well cells, amorphous silicon cells, to name a few. *Zhao et. al*., with the help of optical simulation, showed that by incorporating a-Si:H/ITO stack layers, light absorbance in a 2 µm thick active silicon layer can be enhanced notably [247]. *Isabella et al.* reported that a DBR stack of a-Si:H/SiN_x:H can improve the external quantum efficiency as well as the electrical performance of thin silicon solar cells owing to notable back reflection of light [248]. DBR structures also have the potential of increasing efficiency in multiple-quantum-well (MQW) solar cells fabricated with InGaN/GaN by reflecting longer wavelength photons that were supposed to be transmitted out of the cell [249]. *Banerjee et al.* reported a composite material comprising of Ag_2S nanoparticles embedded in ITO matrix as a back reflector layer for a-Si:H based solar cells [250], which showed significant back reflection in the red and near-infrared region, resulting in about 18% increase in short circuit current density. In our previous work [226], we have reported the fabrication of thin (30 µm) single junction c-Si based solar cells with the help of traditional processing technology that came up with a promising efficiency of 12.25%. Presently, the other advanced

variants of single-junction solar cells that involve crucial optical engineering on the back (like passivated emitter rear contact (PERC) cells) are showing high impact due to their promising future [251-253]. As far as PERC is concerned, it is one of the newest technologies in the solar cell family and currently controlling the research and commercial domain. However, optical management in PERC cells on thin (~30 μm) c-Si has not been reported so far to the best of our knowledge.

In this work, two double dielectric structures comprising two metal oxide stacks of SiO_2/Al_2O_3 and HfO_2/Al_2O_3 have been chosen to explore their light reflection capabilities from the back for both single junction and PERC cells based on thin c-Si substrates. These metal oxides are well known for their passivation and capping applications in PERC cells [254,255]. So, these have been chosen to maneuver the double dielectric layer to minimize the transmittance loss for the higher wavelength lights at the most. Investigations on the carrier generation rate, external quantum efficiency (EQE), and maximum achievable photocurrent density (MAPD) have also been carried out to validate the use of such back reflecting structures in thin c-Si based advanced solar cells.

4.2. Computational modeling and analyses:

4.2.1. Optical Design:

In conventional solar cells, usually, Aluminium is directly deposited as a back contact on a thick c-Si wafer (180 μm) as well as a thin c-Si wafer (~30 μm). Although, Al is a good reflector of visible light, even some portion of it gets transmitted into aluminium and is absorbed in the metal. This may result in Joule heating in the back contact. Though co-fired screen-printed aluminium provides some back-surface field (BSF), it is not a very efficient passivator for advanced solar cells like thin c-Si-based single junction and passivated emitter rear contact (PERC) solar cells. PERC technology

addresses this problem by inserting a passivating dielectric transition metal oxide (TMO) layer between the semiconductor and back contact. The thin passivating dielectric layer is further protected from being penetrated by aluminium during the co-firing process by a capping layer of thick silicon nitride. However, this type of double dielectric layer can be proven to be a very efficient lossless back reflector, more so in the case of solar cells based on thin c-silicon wafers.

For the convenience of analysis and discussion, we have divided the whole structure in two separate domains. Domain 1, as shown in Fig.4.1(a), is constituted of the front SiN_x antireflection coating (ARC) and the bulk silicon. The thickness of the silicon nitride (SiN_x) layer in domain 1 has been selected based on its function as an anti-reflection coating (ARC) on the solar cells. It has been established earlier that this layer exerts the best anti-reflection properties for silicon solar cells when the thickness is about 80 nm [240,256]. So, a thickness of 80 nm has been chosen as the "common standard ARC thickness" for domain 1 in this case. On the other hand, Domain 2, (Fig.4.1(b)) represents the dielectric back reflector. A very thin layer (1nm) of optically lossless silicon (k=0) is assumed on the top of domain 2 to define the Si/Dielectric interface. The back-reflector stack consists of Dielectric 1 (D1)/Dielectric 2 (D2)/Al. Fig.4.1(b) depicts the probable optical path by simply following Snell's law.

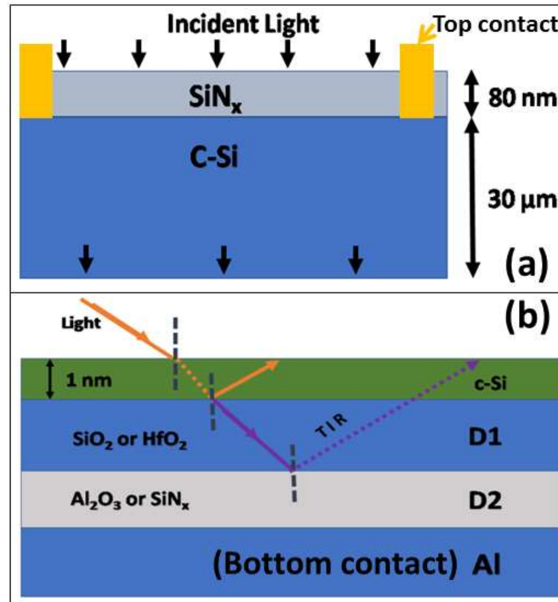

Fig.4.1: Schematic for proposed structure for (a) Domain 1 and (b) Domain 2.

However, if D2 has a lower refractive index than D1, there is a probability of total internal reflection (TIR) of some part of the incident light on the Si/D1 interface, consequently forming a better lossless reflector stack. It is evident from Fig.4.1a that, whenever light falls on the interface-I (air/SiN_x), it bends towards the normal following the Snell's law, whereas; when the light is incident on interface-II (i.e. c-Si/D1) bending takes place away from the normal giving a probability of TIR. The thin (~30µm) silicon wafer is known to transmit light above 700 nm to a great extent. This must be minimized by introducing some back reflector layer to utilize the longer wavelength lights for the enhancement of cell performance.

4.2.2. Modelling and Design Approximation:

For device modelling and computational electromagnetics study, finite element method (FEM) based numerical solver COMSOL^{TM} Multiphysics has been adopted. The Multiphysics solution leaves the opportunity to explore further the scope of investigating

the optoelectronic performance of the proposed device. The Electromagnetic Wave Frequency Domain (EWFD) module has been used to analyze the proposed model here.

As discussed in section 4.2.1 of the paper, the proposed device has a planar structure i.e. it has material homogeneity along two Cartesian axes in three-dimensional Euclidean space. This leaves material inhomogeneity through only one axis that defines the material stack. Such structure can safely be approximated to a two-dimensional (2D) model without losing any significant information. Hence, a 2D model is assumed for the proposed structure for COMSOL simulation, where the material stack is defined along the Y axis. While, along the X axis; the model is assumed to be periodic.

Two ports are defined on the top and at the rear surface of the model to compute the S-parameters and the S-matrices. The port at the top of the simulation domain is named Port 1 and the port at the rearmost end is defined as Port 2. An external source is incorporated at the top port i.e. port 1. The S-parameters can be obtained by computing the surface integral of the functions as presented in the following equations respectively [257].

$$S = \frac{\int_{\partial\Omega}(E - E_1)\cdot E_1}{\int_{\partial\Omega}E_1\cdot E_1} \quad (4.1)$$

$$S = \frac{\int_{\partial\Omega}E\cdot E_1}{\int_{\partial\Omega}E_2\cdot E_2} \quad (4.2)$$

where, E is an excitation electric field, E_1 & E_2 are corresponding electric fields at port 1 and port 2, respectively.

The incident EM wave at port 1 is defined by equation 3.

$$\nabla \times (\nabla \times E) - k_0^2 \varepsilon_r E = 0 \tag{4.3}$$

Where,

$$E(x, y, z) = \tilde{E}(x, y)e^{-ik_z z} \tag{4.4}$$

Here k_0 is the wave number of free space, ε_r is the relative permittivity of the medium k_z is plane wave number and E representsthe electric fieldpropagating along the z-direction.

It must be noted that, although the model is defined in the X-Y plane, the solver considers a continuous homogeneous out of the plane Z-dimension to describe the 3-D wave. The electric field E in the wave equation is a constant vector defined along Z-axis to comply with the continuous boundary condition considering linear polarization. The wave vector k is calculated from frequency or wavelength, elevation angle (α_1), and azimuth angle (α_2).

The present investigation focuses on the performance of the proposed double dielectric structure as the back reflector layer. For this analysis, the light that reaches the Si/BRL interface bears the relevance, which is presented as T(λ). When the light is incident on the Air/Si interface in domain 1, a part of it is reflected back (R(λ)). The rest of it penetrates Si and traverses through its bulk. A part of it gets absorbed in this process which is designated as A(λ). Then T(λ) becomes 1-(R(λ)+ A(λ)). In other words, the reflection loss is inherently included in the estimation of T(λ). The S-parameters in eq. 4.1 and eq. 4.2 also indicates the reflectance part.

The computations are carried out in two parts for two different domains as described in section 4.2.1. For domain 1, the transmittance through the rear surface into

a silicon medium was observed for the wavelength range 300 to 1100nm. This data should give an estimation of the fraction of incident light that reaches the rear surface, and in turn, the Si/ D1 interface. Let this transmittance be T(λ). Now, considering the incident light on the front surface of domain 1 as AM 1.5G defined by the solar energy density spectrum Ph(λ), we can calculate the integrated transmittance T_i as:

$$T_i = \frac{\int_{\lambda 1}^{\lambda 2} Ph(\lambda)T(\lambda)d\lambda}{\int_{\lambda 1}^{\lambda 2} Ph(\lambda)d\lambda} \tag{4.5}$$

In the second part of the present investigation, domain 2 as a back reflector has been assessed by computing the reflectance from the Si/D1 interface, denoted by $R(\lambda)$. Now, integrated back reflectance (R_{bi}) may be calculated with AM1.5G being the incident light at the interface as follows:

$$R_{bi} = \frac{\int_{\lambda 1}^{\lambda 2} Ph(\lambda)R(\lambda)d\lambda}{\int_{\lambda 1}^{\lambda 2} Ph(\lambda)d\lambda} \tag{4.6}$$

R_{bi} provides an objective perspective of the optical response as a back reflector of the proposed dielectric stack for the visible solar spectrum. However, the back reflector does not encounter the AM1.5G solar spectrum; rather, the light transmitted through domain 1 is incident on the Si/D1 interface. Hence, in the context of the proposed structure, the efficiency of the back reflector may be quantified as the integrated reflectance (R_{bt}) as a fraction of the light incident on the top surface of domain 1. The parameter R_{bt} can be calculated by the following equation

$$R_{bt} = \frac{\int_{\lambda 1}^{\lambda 2} Ph(\lambda)T(\lambda)R(\lambda)d\lambda}{\int_{\lambda 1}^{\lambda 2} Ph(\lambda)d\lambda} \tag{4.7}$$

4.3. Results and discussions

4.3.1. Optimization of back reflector layers (BRLs)

The targeted bandwidth for most of the solar cells is 400 – 700 nm, i.e. within the visible region. However, in this case, as the substrate is ~30 µm thick c-Si wafer, it can allow the lights with longer wavelengths (>700 nm) to pass through. For shorter wavelengths (300 – 600 nm), the ~30 µm thick c-Si substrate is quite absorbing. This has been established from the plot of wavelength vs. percentage transmittance within 300 to 1100 nm, as presented in Fig.4.2. This work aims to minimize this loss of light due to transmittance beyond 700 nm by the application of proper back reflecting layers. Within 300–650 nm, there was no notable transmittance from the ~30 µm wafer. A significant rise in transmittance can be observed beyond wavelength 700 nm, resulting in an integrated transmittance T_i (eq. 4.5) of 23.56%.

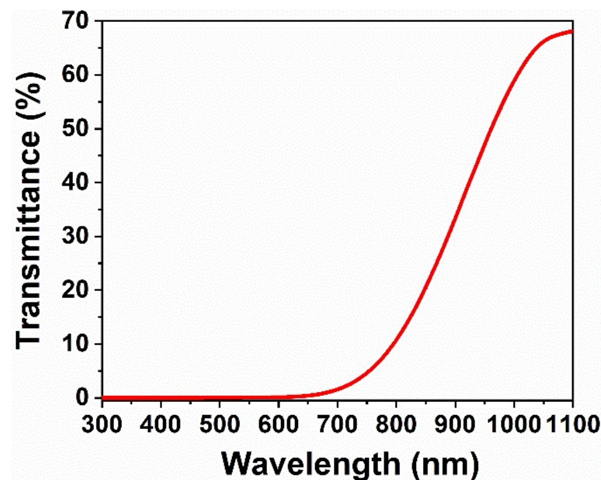

Fig.4.2: Optical transmittance for domain 1 of a ~30 µm thick c-Si wafer.

This significant optical loss needs to be mitigated by the proposed dielectric stack back reflector to enhance the efficiency of the device. Hence, the optoelectronic properties in the present work have been explored within the wavelength range 600 – 1100 nm. In this part of the work, the optical behaviour of the proposed double dielectric stack considering different material combinations with varying thickness has been investigated. As the first

case, the emitter passivated cell structure consisting of 30 µm c-Si as the active layer, and with HfO_2/SiN_x double dielectric layer has been investigated.

In a standard PERC solar cell, metal oxides like HfO_2 or Al_2O_3 are used for rear surface passivation. To protect this passivation layer from metal penetration (while metal co-firing process), a thick layer of SiN_x is used as a capping layer. Here, the thickness of the HfO_2 layer was varied between 2 to 26 nm and the thickness of the SiN_x layer has been varied from 50 to 100nm for this combination. Fig.4.3(a) presents the colormap of integrated reflectance R_{bi} (as per eq. 4.6) and 4.3(b) shows the colormap of R_{bt} for thickness variation of both the dielectric layers.

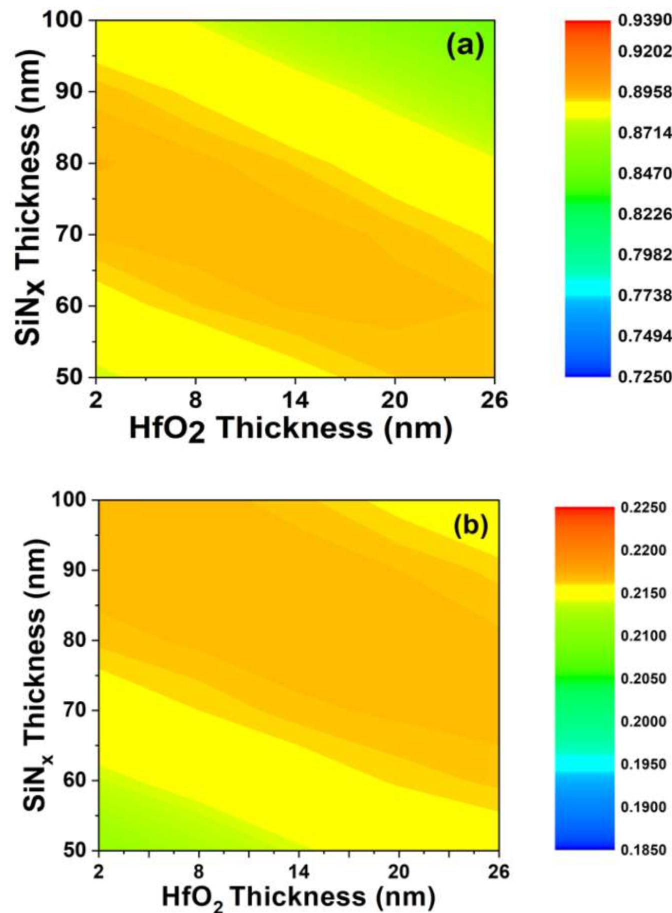

Fig.4.3: Integrated Reflectance plots as a function of dielectric layer thickness for (a) R_{bi} and (b) R_{bt} as obtained from Si/HfO_2 interface by using HfO_2/SiN_x stack as back reflector cum passivator.

It must be noted that both R_{bi} and R_{bt} are dependants on the thickness of both the dielectric layers. The result yielded an optimized thickness of HfO_2 as 14 nm and that for SiN_x is 90 nm.

However, the focus of the present study is on the back reflection properties of dielectric stack structures formed by SiO_2/Al_2O_3 and HfO_2/Al_2O_3 stacks to address the light loss phenomenon through the rear surface of thin c-Si-based advanced solar cells. The thickness variation range of the dielectric layers has been chosen in such a manner to fulfill their primary purposes of passivation and capping considering the practical scenario of cell fabrication. The thickness of the upper SiO_2 layer has been varied widely, from very thin (~1 nm) to moderately thin (~220 nm), to precisely achieve a theoretical sweet point between its thickness and optical properties. For the same reason, the thickness of the HfO_2 layer was varied over a wide range (1 nm to 160 nm). The thickness of the second dielectric layer (Al_2O_3) should be optimized in such a way so that it can act as an optically beneficial capping layer. For this reason, the layer thickness has been varied from 40 to 100 nm, keeping in parity with the variation in conventional SiN_x layer thickness [258]. Similar to Fig.4.3, Fig.4.4(a) and Fig.4.4(b) presents R_{bi} and R_{bt} for $SiO_2/Al_2O_3/Al$ stack structure. The reflectance, in this case, has been monitored at the Si/SiO_2 interface. The color maps of integrated reflectance (R_{bi} and R_{bt}) are presented in Fig.4.4a and 4.4b, respectively.

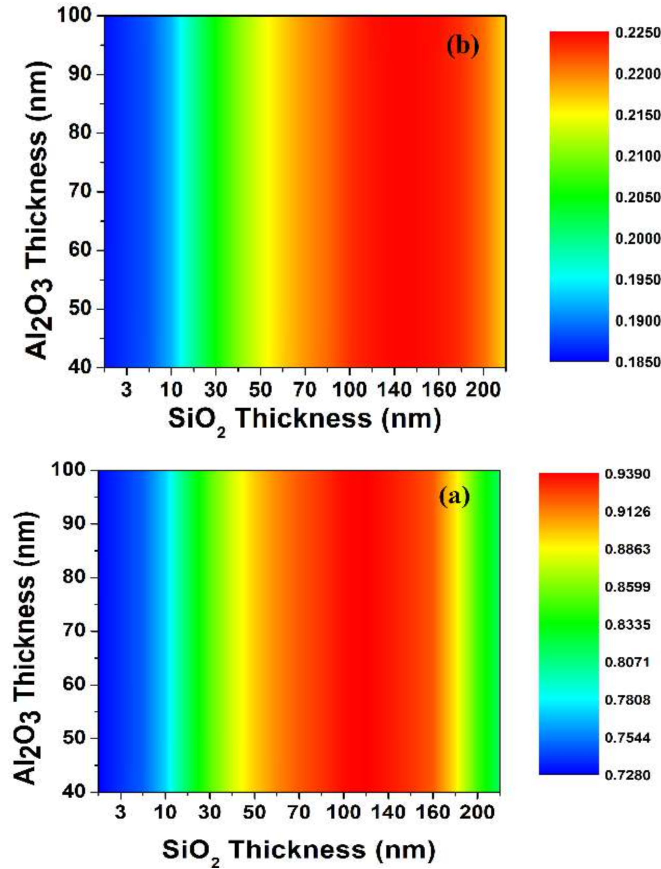

Fig.4.4: Integrated Reflectance plots as a function of dielectric layer thickness for (a) R_{bi} and (b) R_{bt} as obtained from Si/SiO_2 interface by using SiO_2/Al_2O_3 stack as back reflector cum passivator.

It is evident from Fig.4.4 that, neither R_{bi} nor R_{bt} is dependent on the thickness of the Al_2O_3 layer, but their sole dependence is on the thickness of the SiO_2 layer. As the thickness of the SiO_2 layer increases, both R_{bi} and R_{bt} increase until a certain point. After that, both R_{bi} and R_{bt} begin to decrease. This optimal SiO_2 thickness is found to be 120 nm for R_{bi} and 160 nm for R_{bt}. This difference can be explained from the reflectance vs. wavelength (R(λ)) plot shown in Fig.4.5a. These curves directly influence R_{bi} (eq.4.6), whereas, the effect on R_{bt} can be assessed by taking into account the T(λ) spectrum. It can be observed from Fig.5a that, as the thickness of the SiO_2 layer increases up to 120 nm. The magnitude of the trough present in the curves at around 825 nm gets diminished and the reflectance value faces a hike, consequently yielding a higher value for R_{bi}. If the

thickness of the SiO_2 layer goes beyond 120 nm, another valley appears near the wavelength region ~600 nm. Hence R_{bi} reduces beyond this point. This can be seen from the curve for the 200 nm thick SiO_2 layer in Fig.4.5a. For a better understanding of its impact, the area of the valley under a standardized baseline has been calculated and plotted against the thickness of the passivating layer (Fig.4.5b). Here, the area of the valley is a direct indication of the reduction in reflectance. It is evident from the plot (Fig.4.5b) that the area decreases as the thickness of the SiO_2 layer increase up to 120 nm as a result of the reduction in the depth of the valley at ~825 nm. The impact of this improved reflection is visible in the R_{bi} plot in Fig.4.4a. However, beyond the SiO_2 thickness of 120 nm, the appearance of a second valley at the shorter wavelength causes the area of the valley to rise again. This, in turn, results in a reduced reflectance (R_{bi}) for thicker (>120 nm) SiO_2 layers. However, T(λ) is not significantly high in the lower end of the concerned band, so the effect on R_{bt} is not apparent until the said trough moves deeper into the wavelength under consideration. Hence, optimized R_{bt} at a comparatively higher SiO_2 thickness of 140 nm has been obtained. A maximum value of 99.89% has

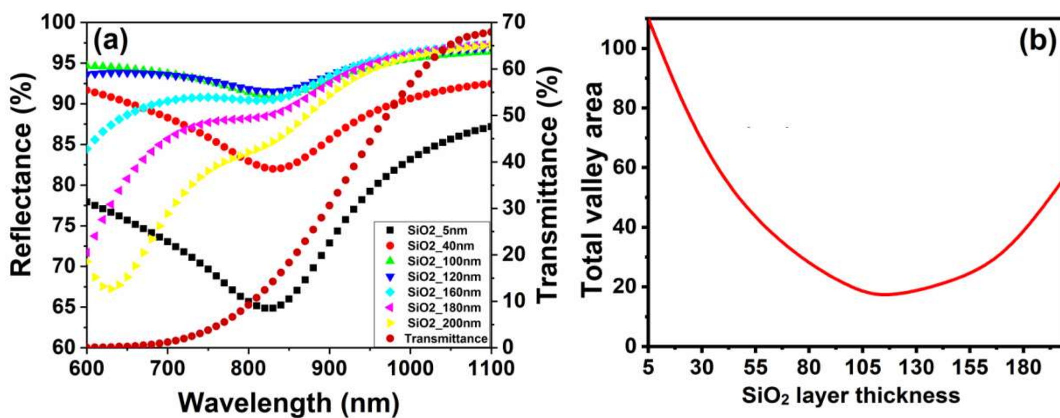

Fig.4.5: (a) Reflectance (R(λ)) plot for different thicknesses of SiO_2 at Si/SiO_2 interface for SiO_2/Al_2O_3 double back reflector layer and (b) plot for variation of a total valley area with SiO_2 layer thickness.

been observed for R_{bi}, whereas R_{bt} produced a maximum value of 22.48% for this SiO_2/Al_2O_3 double back reflector layer on 30μm thin c-Si. An approximated amount of 95% of $T_i$is reflected from the Si/SiO_2 interface and this is quite encouraging. HfO_2 and Al_2O_3 are two important metal oxides and their individual properties have been studied by other groups [259-265] for emitter passivated and other thin silicon solar cells as a back passivation layer. However, the use of a stack or double back reflector cum passivator layer has not been studied in detail so far to the best of our knowledge. In this case, the colormap for R_{bi} and R_{bt} for Si/HfO_2 interface with HfO_2/Al_2O_3 back reflector stacks are presented in Fig.4.6(a) and 4.6(b), respectively. This interface was also found to produce a colormap of a similar pattern as has been obtained for Si/SiO_2back reflector layer. It is evident from Fig.4.6 that the thickness of Al_2O_3 does not play any significant role to alter R_{bi} (88.27%) and R_{bt} (21.44%). The lack of notable dependence of reflectance on the thickness of the Al_2O_3 layer can be attributed to the high reflectance at the SiO_2/Al_2O_3 or HfO_2/Al_2O_3 interfaces. Due to high reflectance at these interfaces, especially at longer wavelengths, a very small fraction of light can penetrate the Al_2O_3 layer and reach the Al_2O_3/Al interface and partially reflected. This reflected light being very small as compared to the light reflected from SiO_2/Al_2O_3 or HfO_2/Al_2O_3 interface, will have a very low impact on overall or integrated reflectance from Si/SiO_2 or Si/HfO_2 interface. Consequently, the thickness of the Al_2O_3 layer will be optically less significant in the performance of the back reflector. Small but indicative variations in the reflectance spectrum with the variation of the thickness of the Al_2O_3 layer can be observed at the longer wavelengths. In addition, similar to the previous stack, both R_{bi} and R_{bt} were found to increase with increasing thickness of the HfO_2 layer in the beginning, and then gradually diminishes beyond a certain value of thickness. However, this optimized thickness of HfO_2 (80 – 100 nm) is found to be lesser than that of SiO_2 (120 – 160 nm).

R_{bi} maximizes at HfO_2 thickness of 80 nm at a value of 88.27%. On the other hand, R_{bt} yielded a maximum value of 21.44% at an optimized HfO_2 thickness of 100 nm.

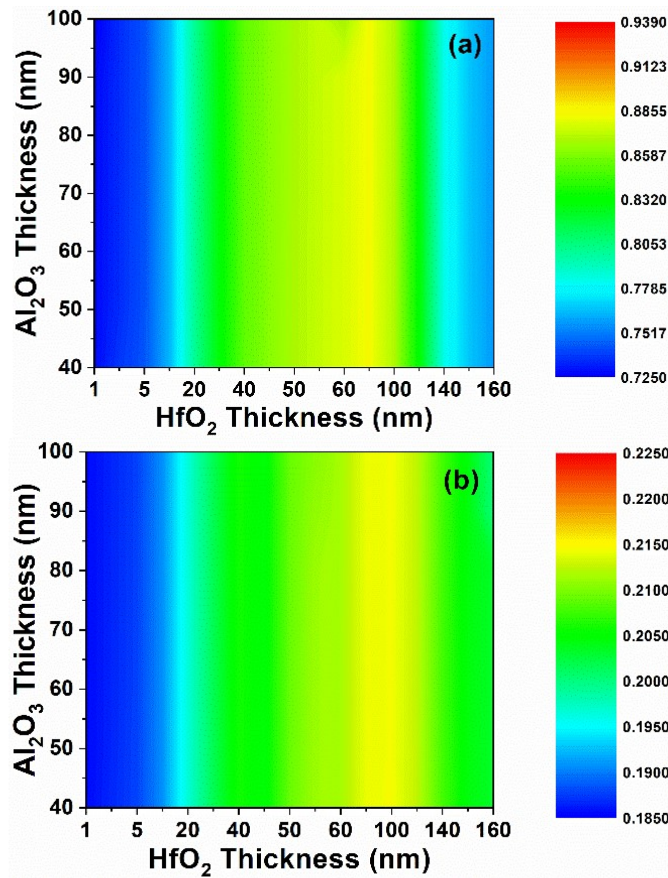

Fig.4.6: Integrated reflectance plots as a function of dielectric layer thickness for (a) R_{bi} and (b) R_{bt} as obtained from Si/HfO_2 interface by using HfO_2/Al_2O_3 stack as back reflector cum passivator.

Again, similar to the previous structure, R_{bi} and R_{bt} vary with the HfO_2 thickness as it appears from Fig.4.7a. This can easily be justified with the help of Fig.4.7a that shows reflectance R(λ) and transmittance T(λ) over a wavelength range of 600 to 1100 nm for this HfO_2/Al_2O_3 stack. Similar to Fig.4.5a, we can see that the trough present in the R(λ) plot reduces as the thickness of HfO_2 increases, thus resulting in improved R_{bi}. However, as the thickness increases beyond 80nm, another trough in the curve comes up with increasing thickness. In this case, also, the impact of the valley can be shown by the change in the area of the valley under a standardized baseline plotted against the thickness

of the HfO_2 layer (Fig.4.7b). Here, the area decreases with increasing thickness of HfO_2 up to 80 nm, as a result of the shallowing depth of the valley presented in Fig.4.7a. The area of the valley, as shown in Fig.4.7b, rises again as the thickness of the HfO_2 layer grows beyond 80 nm, owing to the introduction of the second valley at a shorter wavelength at the higher thickness of the HfO_2 layer. This directly influences R_{bi} by immediately reducing its value for a higher thickness of HfO_2. In this case, the R_{bt} is affected at a higher HfO_2 layer thickness as the trough moves further into the longer wavelength region where T(λ) has enough significant values to have an impact on R_{bt} (eq 4.7). It has been calculated that about 91% of T_i has been reflected from the Si/HfO_2 interface.

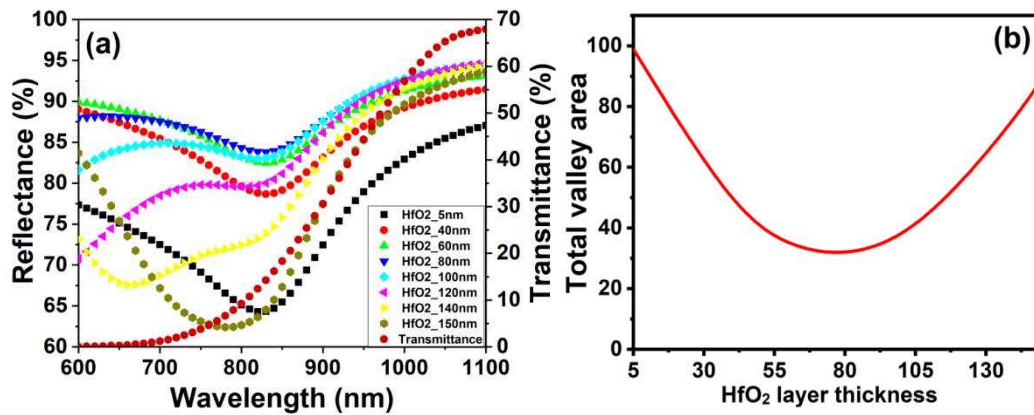

Fig.4.7: Reflectance (R(λ)) plot for different thicknesses of HfO_2 at Si/HfO_2 interface for HfO_2/Al_2O_3 double back reflector layer and (b) plot for variation of a total valley area with HfO_2 layer thickness.

Considering all the results produced above, we can state that the double MO/Al stack can work as a highly efficient lossless back reflector offering reflectance efficiency as high as 95%. Furthermore, comparing the two different material stacks, it has been observed that SiO_2/Al_2O_3/Al stack produces better-integrated reflectances (R_{bi} and R_{bt}) than HfO_2/Al_2O_3/Al structure. Besides, SiO_2/Al_2O_3/Al stack more efficiently reflects

(95%) light from the back surface of the active thin c-Si layer compared to $HfO_2/Al_2O_3/Al$ (91%).

4.3.2. Optoelectronic properties of the BRLs

A detailed theoretical study on the optoelectronic attributes has been carried out to validate the possible practical implementation of the proposed BRLs in thin c-Si based advanced solar cells. Three main parameters that govern the performance of a solar cell, namely, photocarrier generation, external quantum efficiency (EQE), and maximum achievable photocurrent density (MAPD) have been investigated. Photocarrier generation being an explicit function of absorbed power in the medium; is presented as the generation rate per unit volume per unit time as presented in eq.4.8.

$$G(\lambda) = \frac{-0.5|E|^2 Im(\varepsilon)}{\hbar} \tag{4.8}$$

where $G(\lambda)$ is the photocarrier generation rate, E is electric field intensity, ε is the permittivity of the medium and ħ is the reduced Planck's constant.

The generation rate is plotted against the wafer thickness, where the thickness is zero at the rear end and 30 μm at the top. Calculations are done for the p-type c-Si wafer with 30μm thickness, taking standard doping density of 1×10^{16} cm^{-3}. Here, it is worth mentioning that, as the ~30 μm thick c-Si substrate starts transmitting the major portion of light beyond wavelength 600 nm (Fig.1), the optoelectronic properties, in this case, have been explored within the wavelength range 600–1100 nm.

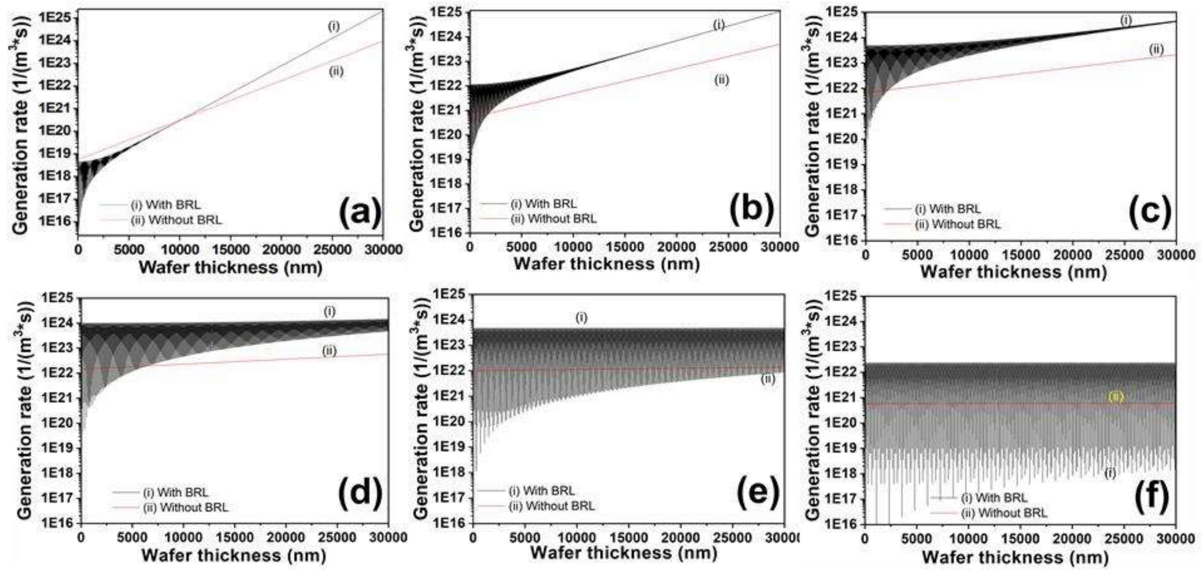

Fig.4.8:Carrier generation rate plotted in $\log_{10}$ scale with respect to wafer thickness at (a) 600 nm (b) 700 nm (c) 800 nm (d) 900 nm (e) 1000 nm and (f) 1100 nm for SiO_2 (140 nm)/Al_2O_3 (100nm) BRL structure.

In each plot of Fig.4.8, curve (ii) represents the generation rate for the device structure without BRL and curve (i) presents the same for the device structure with SiO_2/Al_2O_3 BRL. Fig.4.8a shows the generation rate for the said structure for incident light with wavelength 600 nm. It can be seen from Fig.4.8a that, the generation rate at the rear surface of the wafer (at wafer thickness 0 nm) is quite low, and near the rear end, the nature of curve (i) has some periodicity. Such a lower generation rate is obvious as the field intensity decays exponentially with the depth, resulting in lower carrier generation at the rear surface of the device. However, the periodic nature in the curve (i) appears as a result of the interference pattern created by the superposition of incident light and the reflected light from the Si/SiO_2 interface. The periodic nature dies out within ~5 µm from Si/SiO_2 interface, suggesting the absorption of the reflected light and consequent photocarrier generation. However, for an irradiation wavelength of 600 nm, this interference near the rear surface is effectively more destructive, yielding a lower generation rate as compared to the device without BRL. Nonetheless, the generation rate

near the front surface for a structure with such BRL is found to be greater than that of the structure without BRL in the order of 10^2. This is much significant as the junction depth is about 300nm from the top surface and hence the carriers generated in this region are more likely to be separated in the junction, contributing to an enhancement in photocurrent.

As the wavelength increases, as shown in Fig.4.8b and 4.8c (to 700nm and 800nm respectively), more light reaches the rear Si/SiO_2 interface, resulting in an enhanced carrier generation and thus surpassing the generation rate for a structure without BRL even at the rear end. With further moving towards longer incident wavelengths i.e. 900, 1000, and 1100 nm (as presented in Fig.4.8d, 4.8e, and 4.8f, respectively), it can be seen that a significant part of the back-reflected light reaches the front surface, and multiple reflections between the top and rear surface begin to take place. This can be inferred from the overlapping wave-like features as apparent in plot 4.8e. The overall generation profile within the wafer becomes more uniform at longer wavelengths producing more carriers for this BRL as compared to the structure without BRL. However, at the longer wavelengths of the incident light, the power density in the spectrum reduces; that results in a lowering of the absolute value of generation rate. The maximum generation rate at wavelength 1100 nm for structure with BRL is in the order of 10^{22}. It is evident from the carrier generation profiles as presented in Fig.4.8 that the SiO_2/Al_2O_3 BRL can exploit the lights with longer wavelengths in a better way for a ~30 µm thick c-Si active layer yielding 10 times more carrier generation rate than that of the structure without BRL.

Fig.4.9 represents the carrier generation rate per unit volume per unit time for the HfO_2/Al_2O_3 BRL. Within the chosen active layer, the nature of the carrier generation profile (Fig.4.9a-c) is somewhat similar to that of SiO_2/Al_2O_3 BRL at the shorter wavelengths. However, some finer variations in nature and values at the longer

wavelengths have been observed for HfO_2/Al_2O_3 BRL. The back reflection from Si/HfO_2 interface resulted in interference patterns that are visible in Fig.4.9. The overlapping wave-like feature is attributed to the multiple reflections occurring at longer wavelengths throughout the bulk of the material, as can be observed in Fig.4.9d-f.

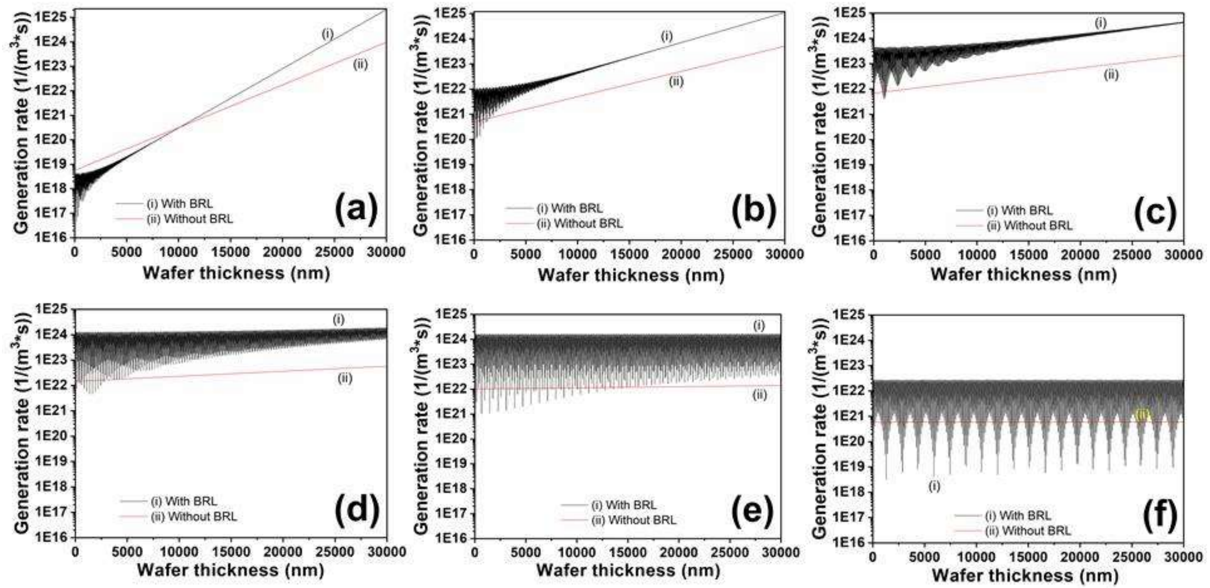

Fig.4.9: Carrier generation rate plotted in $\log_{10}$ scale with respect to wafer thickness at (a) 600 nm (b) 700 nm (c) 800 nm (d) 900 nm (e) 1000 nm and (f) 1100 nm for HfO_2 (100 nm)/Al_2O_3 (100 nm) BRL structure.

It may also be noted that the impact of back reflection is quite similar at shorter (600 and 700 nm) wavelengths for both the BRLs, making the nature of the Figs. 4.8a, 4.8b and 4.9a, 4.9b almost identical in nature. However, comparing the Figs. at wavelengths 800 and 900 nm (Figs 4.9c and 4.9d with 4.8c and 4.8d), it can be noted that the generation rate is considerably larger for SiO_2/Al_2O_3 BRL as compared to HfO_2/Al_2O_3 BRL. On the other hand, from the comparison of the carrier generation profiles at 1000 and 1100 nm (Figs. 4.8e and 4.8f with 4.9e and 4.9f), it can be found that the generation rate for HfO_2/Al_2O_3 is measurably greater than the structure with SiO_2/Al_2O_3 BRL. Hence, it can be inferred that the energy conversion has non-trivial wavelength dependence for these two different BRL structures.

The impact of the photocarrier generation rate for these two proposed BRLs has been measured in terms of maximum achievable photocurrent density (MAPD). The MAPD for a solar cell fabricated on certain material (c-Si with a minority carrier lifetime of 100 μs in this case) can be defined as the short circuit current density (J_{sc}) with no surface recombination and no optical or electrical losses in perfect ohmic contact conditions. The simulation model, in this case, has been chosen to follow these criteria. Hence, the resulting short circuit current density becomes equal to the MAPD. The calculation of MAPD can be carried out in the following way: The total current density (J) is the sum of electron and hole current density (J_n and J_p, respectively).The J_n and J_p are constituted of drift and diffusion currents. The drift and diffusion currents can be calculated from doping concentration and charge carrier density using the following equations:

$$\nabla.(\varepsilon_s \nabla \varphi) = -\rho \quad (4.9)$$

$$\frac{\partial n}{\partial t} = \frac{1}{q}\nabla.J_n - U_n + G_n \quad (4.10)$$

$$\frac{\partial p}{\partial t} = \frac{1}{q}\nabla.J_p - U_p + G_p \quad (4.11)$$

where, ε_s is the permittivity of the medium, φ is the electrostatic potential, n and p are electron and hole concentration, respectively and q is the elementary electronic charge. The recombination rates of electrons and holes are represented by U_n and U_p, respectively. G_n is the electron generation rate and G_p is the hole generation rate. Hence, the charge density ρ can be expressed as:

$$\rho = q(n - p + N_A - N_D) \quad (4.12)$$

where, N_A and N_D are the acceptor and donor doping concentrations, respectively. Hence, electron and hole currents can be calculated from drift and diffusion components, with the help of the following equations:

$$J_n = -q\mu_n n\nabla\varphi + qD_n\nabla n \tag{4.13}$$

$$J_p = -q\mu_p p\nabla\varphi + qD_p\nabla p \tag{4.14}$$

where, μ_n and μ_p represent electron and hole mobility, while diffusion coefficients for them are given by D_n and D_p, respectively.

So, the total current density, which is the measure of MAPD, can be expressed as:

$$J = J_n + J_p \tag{4.15}$$

Fig.4.10 represents the MAPD plotted against the wavelength of the incident light, considering a 30 μm c-Si-based homojunction as the model case. As discussed before, only the longer wavelengths of the incident light reach the rear surface, however, to make a full proof study, 600 to 1100 nm has been chosen to measure the MAPD for both cases. The MAPD has been calculated considering a c-Si wafer with a minority carrier lifetime of 100 μs (to go with the bare minimum case) and otherwise lossless; i.e. no surface recombination and with lossless ideal ohmic contacts. Owing to such a lossless structure, the whole front surface of c-Si can be considered as the front contact and the back aluminium layer as the back contact.

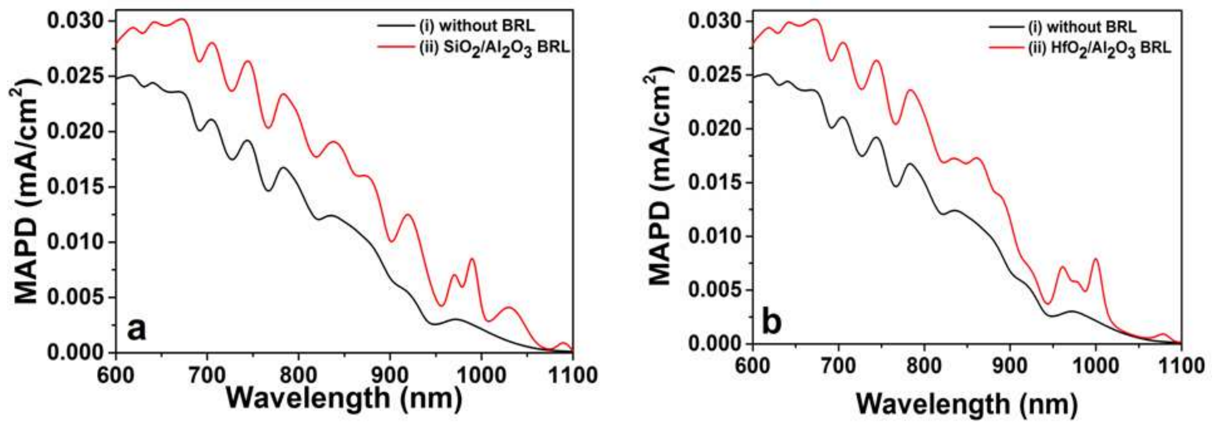

Fig.4.10: Comparison between MAPD of an active layer without BRL and with (a) SiO_2/Al_2O_3 and (b) HfO_2/Al_2O_3 BRLs with optimized thickness.

It can be observed from Fig.4.10 that the MAPD for both the BRLs increases significantly as compared to the active c-Si layer without BRL. However, at shorter wavelengths, the effect of the two different BRLs becomes almost similar towards MAPD. This has good agreement with the carrier generation profiles as has been observed from the Figs. 4.8a,b and 4.9a,b. At the wavelengths beyond 800 nm, the effect of back reflection comes into prominence. Small but distinct effects of the two BRLs are presented in Fig.4.10. The percentage increments in MAPD (concerning no BRL condition) integrated over the entire 600–1100 nm for SiO_2/Al_2O_3 and HfO_2/Al_2O_3BRLs were found to be 41.98% and 35.97%, respectively. These values are quite significant in terms of enhancement in MAPD observed due to efficient (>90%) rear side light management in thin c-Si-based advanced solar cells by the incorporation of the BRLs. As MAPD is resulted from the total absorption of light due to multiple reflections between the front and rear surface of the active layer, its percentage increment is normally higher than the enhancement in R_{bt}. To have an in-depth knowledge, external quantum efficiency (EQE) for the active layer without BRL and with two proposed BRLs at their optimized thickness has been theoretically evaluated and is presented in Fig.4.11. The EQE is defined as the ratio of collected electron-hole pairs to the total incident photons on the solar cells. However, it is calculated as the ratio of the current density to the

maximum possible current density that could have been produced in the case of 100% absorption of the incident photons. The number of photons can be calculated from the incident irradiation as follows:

$$Nph(\lambda) = \frac{Ph(\lambda).\lambda}{hc} \quad (4.16)$$

where, $Nph(\lambda)$ is the number of photons per unit area per unit time, $ph(\lambda)$ is incident irradiation energy per unit area per unit time, λ is the wavelength of the incident light, h is the Planck's constant, $c$is the speed of light in vacuum and q is the charge of an electron.

Now, the external quantum efficiency (EQE) can be expressed as:

$$EQE = \frac{J(\lambda)}{Nph(\lambda).q} \quad (4.17)$$

where, $J(\lambda)$ is the current density obtained from optoelectronic simulation.

Here, the Figs. 4.11a and 4.11b represent the cases for $SiO_2/Al_2O_3$and HfO_2/Al_2O_3 BRLs.

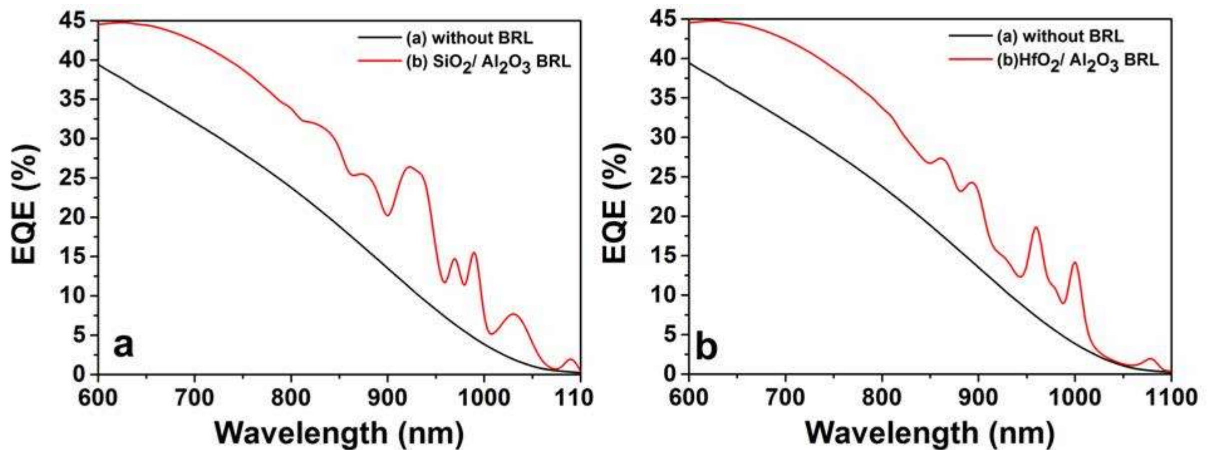

Fig.4.11: Comparison between EQE of active layer without BRL and with (a) SiO_2/Al_2O_3 and (b) HfO_2/Al_2O_3 BRLs with optimized thickness.

In consistence with the MAPD profile (Fig.4.10), the pattern of EQE for the active layers with two different BRLs is indistinguishable at shorter wavelengths. However,

significant enhancement in EQE over 600 – 1100 nm has been observed in both cases in comparison to the EQE of the active layer without any BRL.

4.3.3. Solar cell performance and parameters:

The optical and optoelectronic properties of the proposed BRLs have been discussed at length in Sections 4.3.1 and 4.3.2. To assess any possible gain that might be exerted by the proposed BRLs, simulations on simplified solar cells based on the architectures of the present investigation has been carried out using PC1D. The basic cell (named as S1) was considered to be composed of a homojunction based on a p-type c-Si wafer with a thickness of ~30 μm and a bulk minority carrier lifetime of 100 μs. The junction was formed by front diffusion with a donor doping density of 1×10^{19} cm^{-3}. The top surface anti-reflection coating was considered to be a flat 80 nm [240,256] thick silicon nitride layer as can be seen from Fig.4.1. Ideal ohmic contact was assumed in all cases. Sequentially, computations were done for solar cell structure with proposed BRLs, namely $SiO_2/Al_2O_3/Al$ and $HfO_2/Al_2O_3/Al$ at the rear, named as S2 and S3, respectively. For the cell structure S2, the back reflectance is considered to be 95%, as calculated in Section 4.3.1. The passivation property of the SiO_2 is also taken into account by reducing the surface recombination velocity (SRV) to 80 cm/s [258]. For cell structure S3, the beck reflectance is assumed to be 91%, as per the results obtained from Section4.3.1. The surface passivation is accounted for by the SRV of 55 cm/s [266]. The short circuit current density–voltage (J–V) characteristics of these three cells are plotted in Fig.4.12.

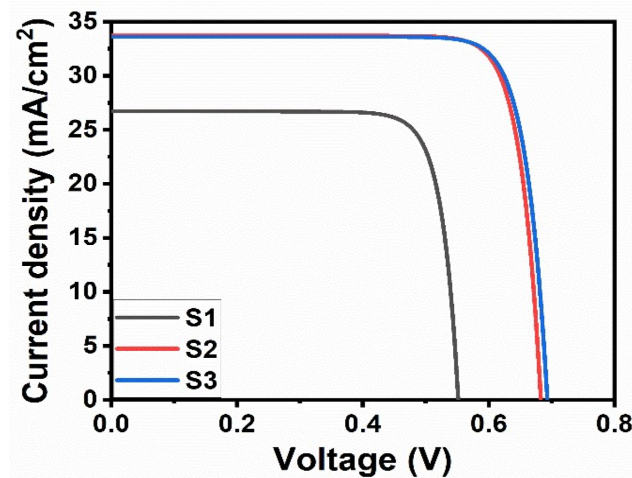

Fig.4.12: Current density – voltage characteristics of the cells with different BRL architectures.

The J–V plot of S1 revealed not so good efficiency of 12.02% with J_{SC}, V_{OC}, and fill factor (FF) of 26.73 mA/cm^2, 0.551V and 81.51%, respectively. For thin wafers, the back aluminium contact is taken through thermal evaporation of the metal. Hence, achieving a good back surface field for the prevention of surface recombination is a bit tricky. As well as, the back reflection of light occurred only due to the metallic attribute of this aluminium layer. This is reflected in the poor cell parameters of S1. It can be observed from Fig.4.12 that the open-circuit voltage for S2 (0.683 V) and S3 (0.693 V) has been improved significantly as compared to S1 (0.551 V). This might be due to the better passivation achieved by the incorporation of the optimized dielectric layers between the c-Si and back Al contact. A significant enhancement in short circuit current density for both S_2 (33.71 mA/cm^2) and S_3 (33.60 mA/cm^2) was also apparent with respect to S1 (26.73 mA/cm^2). The increase in J_{SC} for the case of S_2 and S_3 might be attributed to the enhanced photo generated current, as indicated in Section 4.3.2, and reduced surface recombination losses due to passivation by the introduction of dielectric layers. It is worth mentioning here that the increase in J_{SC} is in good agreement with the increase in MAPD as has been presented

in Section 4.3.2 and Fig.4.10. There was also an improvement in fill factor for S_2 (83.06%) and S_3 (82.76%) than S1 (81.51%). This improvement can be explained with the improved series and shunt resistances (R_{bi} and R_{bt} respectively) for the cells S_2 and S_3. The shunt resistance (R_{sh}) for both S_2 and S3 was obtained ~160kΩ, which is a very significant enhancement as compared to S1 (7.59 kΩ). The effect of surface passivation plays an important role here. However, the series resistance R_s for S_2 and S_3 were found to be around 0.97 and 1.02 Ω, respectively. Although S_3 provides better passivation than S_2, the reflectance provided by the BRL in S_2 is superior to S_3, resulting in greater carrier generation in S_2. It has been established earlier [267] that the series resistance may reduce due to better photocurrent generation. Consequently, S_2 yielded a bit lower series resistance and marginally greater short circuit current as compared to S_3.This resulted in an improved photoconversion efficiency of 19.12% and 19.28% for S_2 and S_3, respectively, i.e. for the cells with SiO_2/Al_2O_3/Al and HfO_2/Al_2O_3/Al BRL architectures.

4.4 Chapter Conclusions

Two double dielectric stack structures, namely, SiO_2/Al_2O_3 and HfO_2/Al_2O_3 have been chosen to investigate their optical performance as a lossless dielectric back reflector for thin c-Si-based advanced solar cell structures. The materials have been identified considering their present individual use as back surface passivator in emitter passivated and other advanced types of solar cells fabricated on thin c-Si. Such devices require good back reflection and light management within the active layer. The thickness of the dielectric layers has been varied to obtain an optimized stack structure yielding maximized integrated reflectance (R_{bi} and R_{bt}). A maximum R_{bt} of 22.48% has been observed for the Si/SiO_2 interface, which is 95% of the light that reaches the bottom surface of the active layer. This has been achieved for a thickness of 140 nm of the SiO_2 layer.

On the other hand, for the HfO_2/Al_2O_3 dielectric stack, the optimized thickness for HfO_2 was found to be about 100 nm that gives a maximum R_{bt} of 21.44%. This constitutes about 91% of the light incident (T_i) on the Si/HfO_2 interface. Carrier generation rate, EQE, and MAPD have been measured that resulted in a significant increment in each of the parameters. Increments in these values were well supported by the enhancement in simulated cell efficiencies. This makes such back reflecting structures worth implementing in thin c-Si based advanced solar cells. These results also suggest that, though SiO_2 requires higher thickness, it is more promising than HfO_2 when used as a passivation cum reflector layer along with Al_2O_3 to function as a double dielectric back reflector layer for thin c-Si-based advanced solar cells.